Tidal Turbine Performance in Sheared Flow

Conor F. Fleming
Dept. of Engineering Science,
University of Oxford,
Parks Road, Oxford, OX1 3PJ, UK
conor.fleming@eng.ox.ac.uk

Simon C. McIntosh*
Dept. of Engineering Science,
University of Oxford
Parks Road, Oxford, OX1 3PJ, UK

Richard H. J. Willden
Dept. of Engineering Science,
University of Oxford
Parks Road, Oxford, OX1 3PJ, UK
richard.willden@eng.ox.ac.uk

***Abstract*—The effect of flow shear on turbine performance and wake development is examined. A computational model of an axial flow tidal turbine is developed and validated, and performance is evaluated in sheared velocity profiles representative of a tidal channel.**

The computational model is developed in the commercial flow solver ANSYS Fluent. The rotor is resolved with a body-fitted grid, which is allowed to rotate relative to the channel boundaries. Symmetry boundary conditions are applied at the sides of the computational domain, simulating an infinite row of turbines. The free surface of the flow is modelled as a rigid lid, by applying a slip condition at the upper surface of the domain. A sheared velocity profile is defined at an upstream boundary and maintained through the specification of shear stress at the channel bed. Validation of this method against scale model experiments is reported.

The device is simulated at various vertical positions in a sheared flow. Rotor thrust and power are observed to increase with elevation above the channel bed. This is a consequence of the higher kinetic flux in upper portion of the velocity profile.

Further, it is found that using an alternative normalisation for thrust and power, based on the upstream velocity profile in place of a single reference velocity, enables collapse of results across a range of sheared profiles.

I. Introduction

Tidal turbines operate in more highly sheared flows than wind turbines. The level of shear can be quantified by the ratio of roughness length y_0 to boundary layer height h. Roughness length is defined in the logarithmic law of the wall,

$$u = \frac{u_\tau}{\kappa} \ln \frac{y}{y_0} \tag{1}$$

$$u_\tau = \sqrt{\frac{\tau_w}{\rho}}, \tag{2}$$

where u is velocity, u_τ is friction velocity, $\kappa = 0.41$ is the von Kármán constant, y is the vertical coordinate, τ_w is the wall shear, and ρ is the density of the fluid [1]. y_0 is the location where the extrapolated function from equation 2 intersects with the axis $u = 0$. Typical published values for roughness height from wind velocity profiles are compared to calculated roughness values for the tidal velocity profiles from section II-A in table I.

A consequence of the higher shear in tidal flows is that tidal turbine rotor blades must withstand a greater fatigue load associated with rotation. Additionally, the turbine should be positioned away from the sea bed in order to encounter the higher kinetic flux in the upper portion of the flow.

TABLE I
Scaled roughness heights for wind and tidal flows.

Profile	y_0 [m]	h [m]	y_0/h
Wind	0.01 - 0.25 [2]	1000 [3]	1×10^{-5} - 2.5×10^{-4}
Tidal	0.03 - 0.14	46.5	6×10^{-4} - 3×10^{-3}

A computational model is developed using the Reynolds averaged Navier Stokes equations (RANS) solver ANSYS Fluent [4] to explore the performance of tidal turbines in sheared flow. Resolution of the rotor geometry via a body-fitted grid is necessary to explore the resulting fluctuations in blade forces, which will be the focus of future work. In this paper, we present a validation of the model against a scaled experiment, and simulate a full scale turbine operating at different elevations in a sheared flow, to highlight the effect on power generation. We also show how turbines operating in differently-sheared flows may be compared directly through appropriate normalisation of performance parameters.

II. Open channel flow

One difficulty encountered in RANS modelling of highly turbulent flows (where turbulence intensity, $TI \approx 10\%$), is that turbulent kinetic energy prescribed at the domain inlet boundary decays quickly as the flow develops downstream. Here we describe a method of preventing such decay. A fully-developed velocity profile is prescribed, with matching profiles of turbulent kinetic energy, k, and specific dissipation rate, ω. The sheared velocity profile provides a mechanism for continuous local production of turbulence, sustaining a relatively high turbulence flow throughout the computational domain.

A. Derivation of sheared flow profiles

Analytical profiles of streamwise velocity, u, turbulent kinetic energy, k, and specific dissipation rate, ω, are derived following Schlichting [1], and compared to measurements from a tidal channel. The velocity profile is set via a bed roughness coefficient, c_f, and a reference velocity u_{nom} (defined formally

*Now at Culham Centre for Fusion Energy, Culham Science Centre, Abingdon, Oxfordshire, OX14 3DB, UK

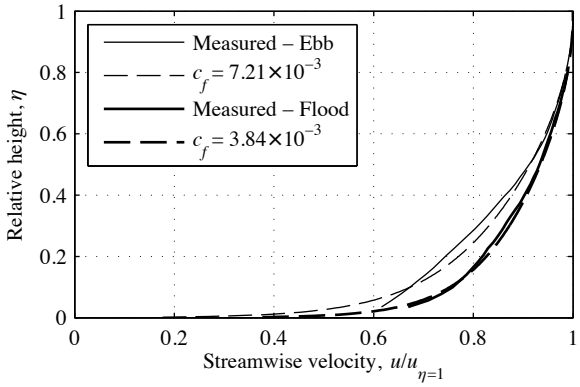

Fig. 1. Comparison of measured (solid lines) and analytical (broken lines) velocity profiles for a tidal channel.

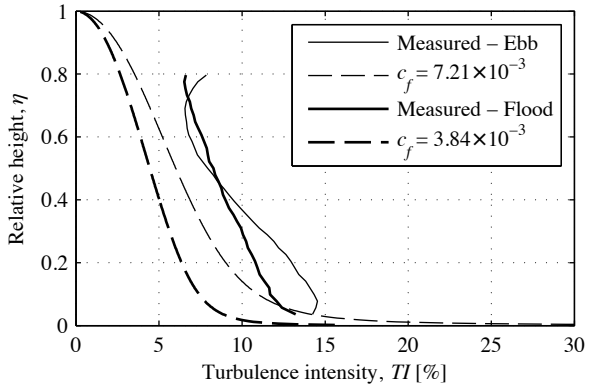

Fig. 2. Comparison of measured (solid lines) and analytical (broken lines) turbulence intensity profiles for a tidal channel.

in equation 8). The friction velocity, u_τ, is defined as

$$u_\tau = u_{\text{nom}}\sqrt{\frac{c_f}{2}}, \tag{3}$$

from which the applied bed shear, τ_{w}, is calculated,

$$\tau_{\text{w}} = \rho u_\tau |u_\tau|. \tag{4}$$

The velocity distribution is assumed to take the form of one half of a fully developed Poiseiulle flow profile, where there is a linear variation in shear force from a maximum of τ_{w} at the channel bed to a minimum of $\tau = 0$ at the free surface. This shear profile may be expressed as a function of dimensionless depth, $\eta \equiv y/d$, where h is water depth,

$$\tau(\eta) = \tau_{\text{w}}(1-\eta) = \rho\nu_{\text{t}}\frac{\text{d}u}{\text{d}\eta}\frac{\text{d}\eta}{\text{d}y}. \tag{5}$$

Taking the ansatz for turbulent eddy viscosity [1], [5],

$$\nu_{\text{t}} = \frac{1}{6}u_\tau d\kappa\left[1-(1-\eta)^2\right]\left[1+2(1-\eta)^2\right], \tag{6}$$

equation 5 can be integrated to yield the velocity profile for a turbulent Poiseuille flow,

$$u(\eta) = \frac{u_\tau}{\kappa}\ln\left(\frac{\eta(2-\eta)}{2\eta^2-4\eta+3}\right) + u_d \tag{7}$$

where $\kappa = 0.41$ is the von Kármán constant and u_d is the streamwise velocity at the free surface.

The reference flow velocity (used previously in equation 3) is defined as the average of the velocity profile,

$$u_{\text{nom}} = \int_0^1 u(\eta)\text{d}\eta, \tag{8}$$

which is solved for u_d,

$$u_d = u_{\text{nom}} - \overline{c}, \tag{9}$$

where

$$\overline{c} = \frac{u_\tau}{\kappa}\left(\ln\frac{4}{3} - \frac{\pi}{\sqrt{2}} + \sqrt{2}\arctan\frac{1}{\sqrt{2}}\right). \tag{10}$$

The profile of turbulent kinetic energy, k, resulting from this velocity distribution is calculated using the one-equation turbulence model of Bradshaw et al. [6],

$$k = \frac{\tau_{\text{t}}}{a\rho} = \frac{u_\tau^2(1-\eta)}{a}, \tag{11}$$

where $a = 0.3$ is a turbulence constant. Subsequently, a profile of specific turbulence dissipation rate, ω, may be calculated [1],

$$\omega = \frac{k}{\nu_{\text{t}}}. \tag{12}$$

The profile of turbulence intensity, TI, is also calculated from the profile of turbulent kinetic energy,

$$TI = 100\sqrt{\frac{2}{3}k}. \tag{13}$$

B. Comparison to measured data

Profiles of velocity and turbulence intensity are now compared to acoustic Doppler current profiler (ADCP) data from a representative tidal site. Profiles of mean streamwise velocity, u, are calculated from raw velocity data sampled at 1 Hz over one full tidal cycle, where the depth is approximately 46.5 m and peak velocities of 2.03 m s^{-1} and 2.28 m s^{-1} are observed for the ebb and flood tides respectively. Periods of slack tide (when $u < 0.75$ m s^{-1}) are discounted from the signal before averaging. As discussed earlier, the modelled velocity profile is governed by the bed friction coefficient, c_f. Representative values for bed friction coefficient were found by fitting the analytical velocity profile to the field data. Figure 1 shows that good fits are achieved between measured and analytical velocity profiles with bed friction coefficients of $c_f = 0.00384$ (flood) and $c_f = 0.00721$ (ebb).

Turbulence intensity was calculated from the unsteady velocity signal over the same periods,

$$TI = \frac{\sqrt{\frac{1}{3}\left(u'^2+v'^2+w'^2\right)}}{U}, \tag{14}$$

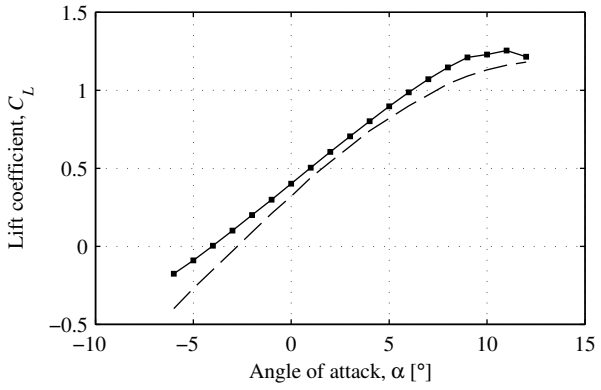

(a)

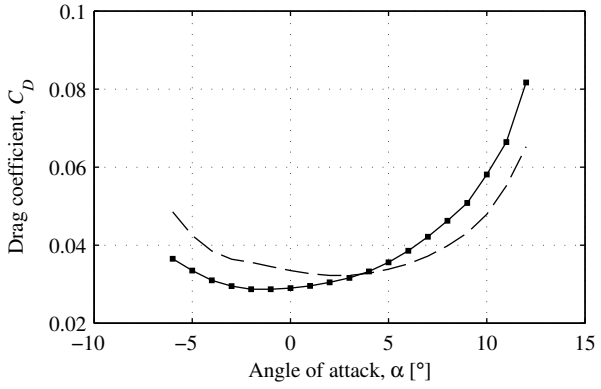

(b)

Fig. 3. Comparison of computed (solid line with square markers) and experimental [7] (broken line) sectional forces for a NACA 4415 profile at $Re = 42 \times 10^3$.

where u', v' and w' are velocity fluctuations in the x, y and z directions respectively, and U is the magnitude of the mean velocity. Turbulence intensity profiles calculated from the raw velocity signal are very sensitive to the cutoff timescale. Good agreement with the analytical turbulence intensity profile is achieved for cutoff timescales of under 10 seconds; however the frequency of the raw data is only 1 Hz. A demonstrative comparison of turbulence profiles for a cutoff timescale of 1 minute is presented in figure 2.

III. Normalisation of performance parameters

Tidal turbine performance is conventionally reported in terms of thrust and power coefficients, C_T and C_P,

$$C_T = \frac{T}{\frac{1}{2}\rho A_\mathrm{r} u_\mathrm{ref}^2};\; C_P = \frac{P}{\frac{1}{2}\rho A_\mathrm{r} u_\mathrm{ref}^3}, \tag{15}$$

where ρ is the density of the fluid, A_r is the swept rotor area and u_ref is a reference velocity.

The operating point of a turbine is conventionally reported in terms of tip speed ratio,

$$\lambda = \frac{u_\mathrm{tip}}{u_\mathrm{ref}} \tag{16}$$

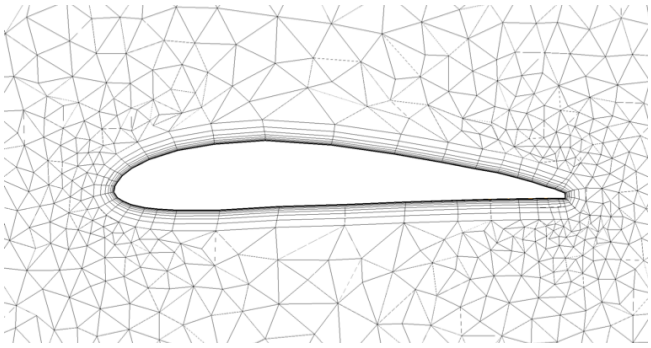

Fig. 4. Cutplane through the model scale computational domain showing mesh resolution in the vicinity of the rotor blade at the 80% radial station.

where the tip velocity of the blade is defined as $u_\mathrm{tip} = \omega R$ and R is the rotor radius.

For comparison of turbines in sheared flow, we propose alternative definitions of thrust and power coefficients which take the level of flow shear into account. The distributed thrust on the rotor can be normalised by the second moment of the upstream velocity profile (area-average of velocity squared),

$$C'_T = \frac{T}{\frac{1}{2}\rho \int_{A_\mathrm{r}} \left[u_\infty(y,z)\right]^2 \,\mathrm{d}A}, \tag{17}$$

where the integration is performed on the undisturbed profile far upstream of the rotor over the area which is intersected by the projected swept area of the rotor, A_r. Similarly, power can be normalised by the third moment of the upstream profile,

$$C'_P = \frac{P}{\frac{1}{2}\rho \int_{A_\mathrm{r}} \left[u_\infty(y,z)\right]^3 \,\mathrm{d}A}. \tag{18}$$

A new tip speed ratio should now be used in conjunction with C'_T and C'_P,

$$\lambda' = \frac{u_\mathrm{tip}}{\frac{1}{A_\mathrm{r}} \int_{A_\mathrm{r}} u_\infty(y,z)\,\mathrm{d}A} \tag{19}$$

These alternative performance coefficients enable direct comparison of turbines operating in different velocity profiles, as will be demonstrated in section VI.

IV. Computational model

A. Introduction

Two computational models are presented in this paper. The first is matched to a physical experiment at a geometrical scale of 1 : 30. The second model is a full-scale representation of a tidal turbine, and is used to investigate turbine performance in sheared flows. Details of both models are given in the following sections.

B. Geometry

The experimental scale turbine features a three-bladed axial flow rotor, with diameter of 0.6 m, and a NACA 4415 blade section. Note that this aerofoil section has been chosen because due the availability of experimental data at low

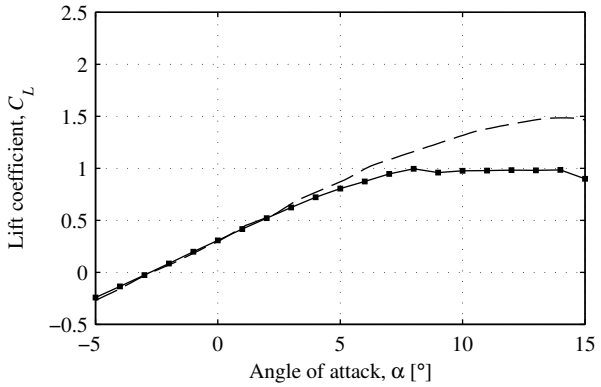

(a)

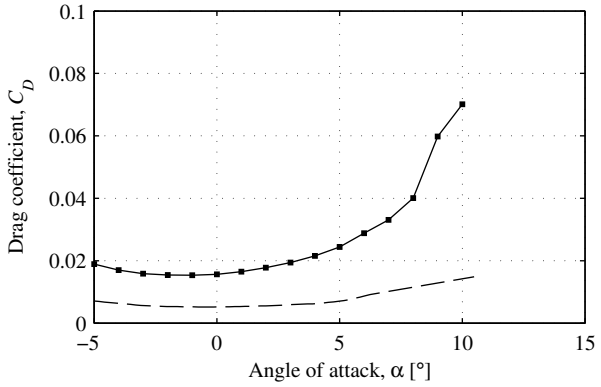

(b)

Fig. 5. Comparison of computed (solid line with square markers) and experimental [9] (broken line) sectional forces for a NACA 63_3-418 profile at Re = 6×10^6.

Reynolds numbers (see section IV-C). The centrebody is approximately cylindrical, with a diameter of 0.085 m, and a rounded nose. The total length is approximately 0.65 m. The turbine is supported from above by a surface-piercing tower of diameter 0.04 m. The device is tested in a recirculating flume of width 1.5 m depth of 0.8 m and nominal velocity of $u_{\text{nom}} = 0.41\,\text{ms}^{-1}$ at mid-depth. The resulting area blockage, defined as the ratio of the swept area of the rotor to the cross-sectional area of the channel, is $B \approx 23.6\%$.

The full scale turbine geometry has been provided by the PerAWaT consortium [8] and is illustrated in figure 7. It features a three-bladed axial flow rotor with a diameter of $D = 18$ m. The blade section is based on a NACA 63_3-4xx aerofoil, where the thickness xx ranges from 55% at the root to 18% at the tip. The centrebody consists of a spinner and a nacelle, with a diameter of 3 m and total length of approximately 10 m. The spinner has a semi-ellipsoidal form with a major-to-minor axis ratio of 1.5 : 1. The turbine is supported from below by a cylindrical monopile of diameter 2 m which is fixed to the channel bed.

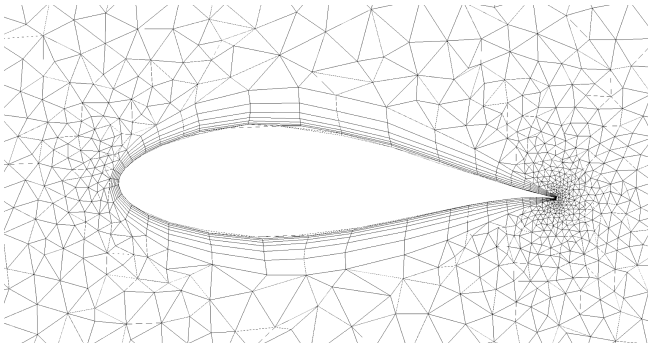

Fig. 6. Cutplane through the full scale computational domain showing mesh resolution in the vicinity of the rotor blade at the 80% radial station. Note that the blade section at this station is equivalent to a NACA 63_3-426.

C. Spatial discretisation

The domain is discretised into an unstructured body-fitted grid of predominantly tetrahedral elements. For both the experimental scale and full scale models, appropriate resolution in the vicinity of the rotor is determined through a mesh sensitivity study on a two-dimensional aerofoil section. Flow conditions for this study are set so as to represent local blade conditions when the turbine is in operation, and to match available wind tunnel data.

The experimental scale mesh resolution study is carried out on a NACA 4415 aerofoil at a Reynolds number of $\text{Re} \approx 42 \times 10^3$. Twelve layers of high aspect ratio prismatic elements are used to resolve the boundary layer. A non-dimensional wall distance of $y^+ \approx 1.0$ is set for the centroids of the first layer of prism elements, and the height of subsequent layers increases by a factor of 1.5. Plots of lift coefficient, $C_L = L/\frac{1}{2}\rho u_\infty^2 c$ (where c is chord length) and drag coefficient, $C_D = D/\frac{1}{2}\rho u_\infty^2 c$ are displayed in figures 3(a) and 3(b), with comparison to experimental data at the same Reynolds number [7].

A cutplane through the rotor mesh in the corresponding three-dimensional computational domain is presented in figure 4. Based on this resolution study, and the capacity of the available computing resource, the maximum tetrahedral element dimension is set at $0.5c$ in the vicinity of the turbine and tower (near field region), and is $0.625c$ in the far field, where c is the chord length at the 80% radial station.

For the full scale turbine, the blade section Reynolds number at the 80% radial station is $\text{Re} \approx 7.2 \times 10^6$. At such a high Reynolds number, the available computational resource is not capable of simulating a full three dimensional turbine geometry with fully resolved boundary layers. Instead, wall functions are used to model the boundary layers, enabling a wall-adjacent cell height of $100 < y^+ < 500$ to be set for the centroids of the first layer of prism elements. 6 layers of prism elements with a growth factor of 1.5 line the turbine surfaces. Computed lift and drag forces on the NACA 63_3-418 section are compared to experimental measurements [9] in figures 5(b) and 5(a).

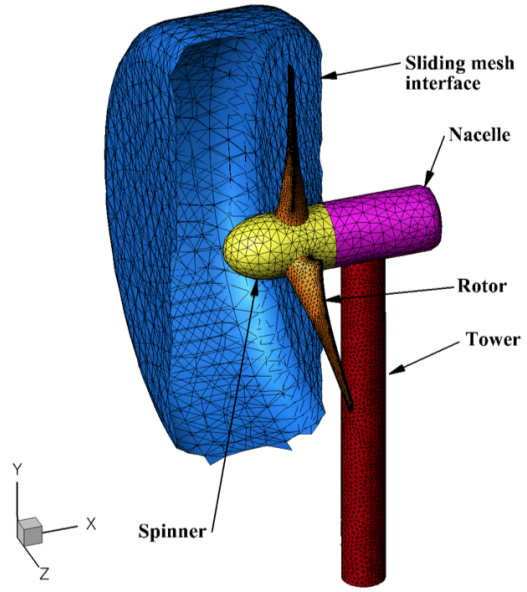

Fig. 7. Isometric view of the surface mesh on the turbine geometry and the sliding mesh interface.

A cutplane through the rotor mesh in the corresponding three-dimensional computational domain is presented in figure 6. The maximum tetrahedral element size in the near field region is $1.0c$, and in the far field region is $2.0c$.

D. Computational Setup

1) Turbulence Model: The k-ω SST turbulence model is used. Profiles of turbulent kinetic energy k and specific dissipation rate ω are set based on the velocity profile, following equations 11 and 12 respectively.

2) Velocity Profile: The open channel flow velocity and turbulence profiles developed in section II-A are not used at experimental scale, as the flume flow exhibits shear from the sides as well as the bed. The measured velocity profile is approximated by blending horizontal and vertical log law functions, and matching the volumetric flow rate to that of the flume. A wall roughness height of $z_o = 6.12 \times 10^{-5}$ m has been calculated by fitting a one-dimensional log law profile to the velocity profile measured at the vertical midplane of the flume. The velocity at mid depth in the flume is $0.41\,\mathrm{ms}^{-1}$.

For the full scale computational model, the velocity profile developed in section II-A is used.

For both computational models, the inlet boundary is located three rotor diameters upstream of the rotor plane.

3) Free Surface: The free surface is modelled as a rigid lid in the experimental scale and full scale models.

4) Downstream Boundary: In both models, a constant pressure of 0 Pa is prescribed across the outlet of the domain, which is located 6 diameters downstream of the rotor plane.

5) Lateral Boundaries: As described in section IV-D2, a rough wall boundary condition is applied at the sides as well as the bed of the experimental scale computational domain.

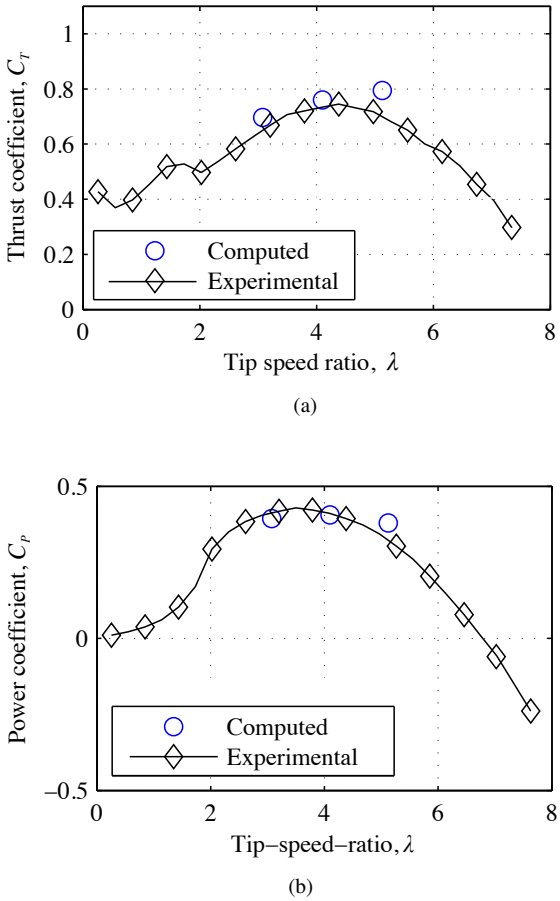

Fig. 8. Comparison of computed and measured thrust for the model scale turbine.

The focus of the full scale model is on turbine performance in a vertically-sheared profile. Symmetry boundary conditions are applied at the lateral boundaries of the full scale domain to simulate an infinite row of contra-rotating turbines.

6) Sliding Mesh: A sliding mesh interface is used to enable angular motion of the rotor relative to the domain boundaries. The rotor and spinner are enclosed within a cylindrical region, illustrated for the full scale turbine in figure 7. The interface boundary is lined with non-conformal surface meshes of two-dimensional triangular elements on either side.

For the experimental scale simulation, the rotor advances 0.6° every timestep, while for the full scale model the rotor advances 2° every timestep.

V. Comparison to Experiment

The 1 : 30 scale turbine is simulated at tip speed ratios of 3, 4 and 5. The numerical and experimental models are compared in figure 8. Power is slightly under-predicted at $\lambda = 3$, and over-predicted at $\lambda = 5$. This is consistent with the sectional blade drag in figure 3(b). At lower tip speed ratios, the angle of attack is higher. Blade drag is over-predicted, with a detrimental effect on rotor power. The opposite is the case

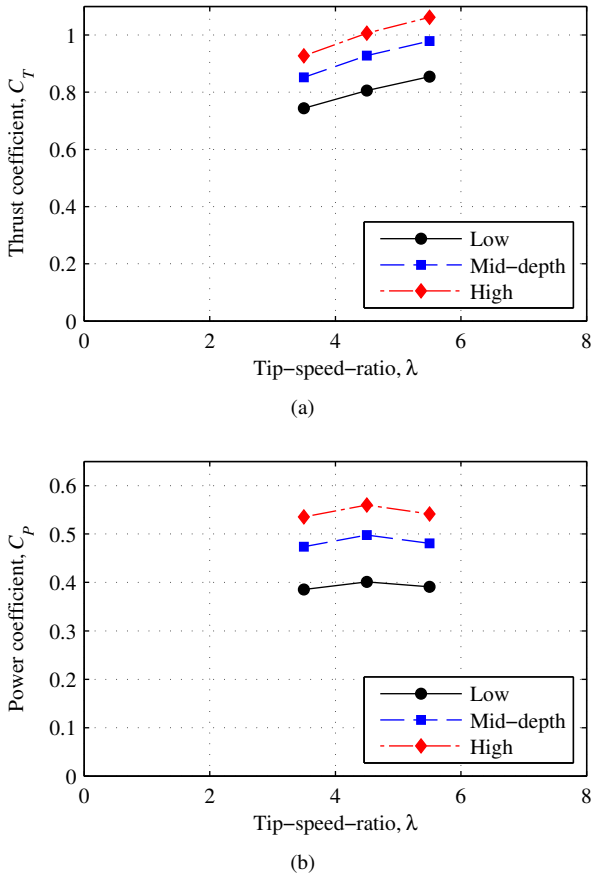

Fig. 9. Effect of elevation on turbine performance.

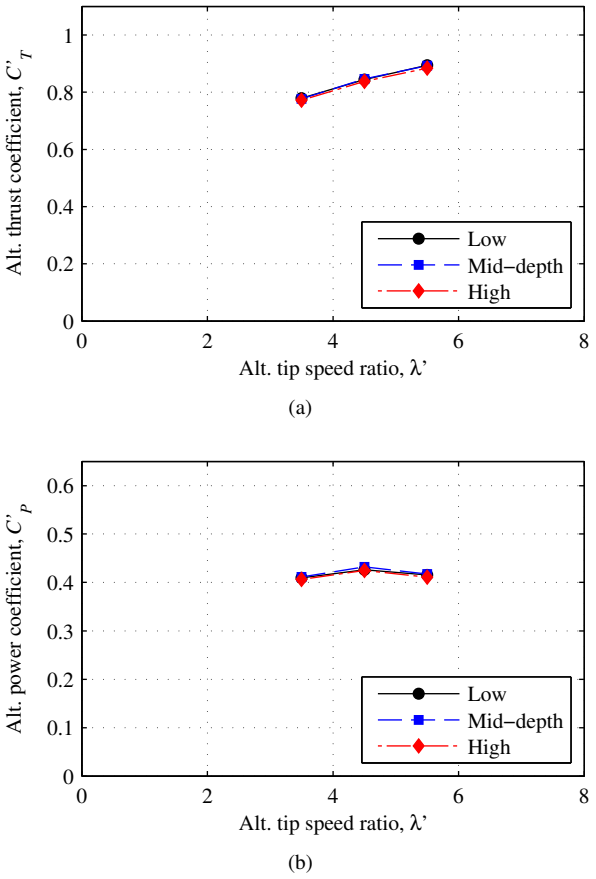

Fig. 10. Comparison of turbines at different elevations from figure 9 with renormalised performance coefficients.

at higher tip speed ratios, resulting in over-prediction of rotor power.

VI. Full scale operation in sheared flow

The turbine is modelled at three heights in a sheared flow: close to the channel bed, at mid-depth and close to the free surface. Upstream profiles of velocity and turbulence parameters are set following section II-A. A bed friction coefficient of $c_f = 0.007$ is used, which is close to that observed on the ebb tide at a typical tidal site (see figure 1). The heights are expressed in terms of the water depth h in table II. The turbine is simulated at tip speed ratios of 3.5, 4.5 and 5.5.

TABLE II
Turbine hub elevation

Elevation	y/h
Low	0.35
Mid-depth	0.5
High	0.65

A. Thrust and power performance

Blade forces are monitored during the simulation. The flow field is deemed to be temporally converged when the blade forces become periodic. Power and thrust coefficients are then calculated by integrating rotor forces over three subsequent revolutions.

Rotor power and thrust coefficients are compared for the three turbine elevations in 'flood' shear conditions in figures 9(a) and 9(b). The highest values of thrust and power are observed for the high elevation case, $y/h = 0.65$. This is because the rotor encounters higher velocity flow in the upper portion of the sheared velocity profile.

Figure 9(b) indicates that a turbine should be sited away from the bed of a tidal channel for best power performance. However, the increased thrust at high elevation, highlighted in figure 9(a), necessitates a stronger (and thus more expensive) supporting structure. Hence a trade-off exists between support structure cost and increased revenue from higher power generation.

B. Renormalisation for sheared flow

The effect of flow shear can be accounted for through appropriate normalisation of thrust and power coefficients as

described in section III. This enables a fairer comparison to be made between different turbines operating in velocity profiles.

We now repeat the comparison of turbines in sheared flow at different elevations, using the new definitions of power and thrust coefficient. The respective thrust and power curves collapse, showing that showing that the differences in upstream velocity profile are properly accounted for. This result indicates that turbine performance in a given velocity profile can be predicted based on knowledge of performance in a different velocity profile, including uniform flow.

VII. Conclusion

The RANS solver ANSYS Fluent has been used to investigate the performance of tidal turbines in a sheared velocity profile. Suitable sheared profiles have been generated from velocity measurements at a representative tidal site. The issue of turbulence decay in the free stream of RANS models is mitigated by prescribing a fully developed open channel flow velocity profile with matched profiles of turbulence kinetic energy and dissipation rate, which are maintained through the application of bed shear. Comparisons in performance with a 1 : 30 scale model experiment show good agreement in thrust and power coefficients, with explicable differences due to discrepancies in predicted sectional drag.

Simulations are carried out on a full scale tidal turbine at various heights in sheared flows. It is observed that turbine performance in a sheared flow is improved with increased elevation.

Finally, the effects of flow shear may be accounted for through normalisation of rotor thrust and power on the second and third moments of the upstream velocity profile. This new normalisation provides a mechanism through which turbine performance in sheared flow may be assessed based on knowledge of performance in unsheared conditions.

In future work, the blade forces will be analysed to determine the fatigue loading due to turbine operation in sheared flow.

Acknowledgment

This work was undertaken as part of the PerAWaT project, which was commissioned and funded by the Energy technologies Institute (ETI).

References

[1] H. Schlichting, *Boundary Layer Theory*, 8th ed. Springer-Verlag, 2000.

[2] J. Wieringa, "Updating the davenport roughness classification," *Journal of Wind Engineering and Industrial Aerodynamics*, vol. 41, no. 1–3, pp. 357 – 368, 1992. [Online]. Available: http://www.sciencedirect.com/science/article/pii/016761059290434C

[3] M. Calaf, C. Meneveau, and J. Meyers, "Large eddy simulation study of fully developed wind-turbine array boundary layers," *Physics of Fluids*, vol. 22, no. 1, p. 015110, 2010. [Online]. Available: http://link.aip.org/link/?PHF/22/015110/1

[4] ANSYS, Inc., *ANSYS FLUENT User's Guide*, ANSYS, Inc., 275 Technology Drive Canonsburg, PA 15317.

[5] K. Gersten and H. Herwig, *Strömungsmechanik: Grundlagen der Impuls-, Wärme- und Stoffübertragung aus asymptotischer Sicht*. Vieweg Verlagsgesellschaft, 1992.

[6] P. Bradshaw, D. H. Ferriss, and N. P. Atwell, "Calculation of boundary-layer development using the turbulent energy equation," *Journal of Fluid Mechanics*, vol. 28, pp. 593–616, 1967.

[7] S. J. Miley, "A catalog of low Reynolds number airfoil data for wind turbine applications, DE82-021712," National Technological Information Service, Tech. Rep., 1982.

[8] R. Rawlinson-Smith, I. Bryden, M. Folley, V. Martin, T. Stallard, C. Stock-Williams, and R. Willden, "The PerAWaT project: Performance Assessment of Wave and Tidal Array Systems," in *Proc. 3rd International Conference on Ocean Energy (ICOE), Bilbao, Spain.*, 2010.

[9] I. H. Abbott and A. E. Von Doenhoff, *Theory of wing sections, including a summary of airfoil data*. Dover Publications, 1959.